# An Electronic Perspective on the Reduction of an N=N Double Bond at a Conserved Dimolybdenum Core

**Julia K. Padden Metzker and John E. McGrady*[a]**

**Abstract:** Density functional theory has been used to assess the role of the bimetallic core in supporting reductive cleavage of the N=N double bond in $[Cp_2Mo_2(\mu\text{-}SMe)_3(\mu\text{-}\eta^1{:}\eta^1\text{-}HN{=}NPh)]^+$. The HOMO of the complex, the Mo–Mo δ orbital, plays a key role as a source of high-energy electrons, available for transfer into the vacant orbitals of the N=N unit. As a result, the metal centres cycle between the $Mo^{III}$ and $Mo^{IV}$ oxidation states. The symmetry of the Mo–Mo δ "buffer" orbital has a profound influence on the reaction pathway, because significant overlap with the redox-active orbital on the N=N unit (π* or σ*) is required for efficient electron transfer. The orthogonality of the Mo–Mo δ and N–N σ* orbitals in the $\eta^1{:}\eta^1$ coordination mode ensures that electron transfer into the N–N σ bond is effectively blocked, and a rate-limiting $\eta^1{:}\eta^1 \rightarrow \eta^1$ rearrangement is a necessary precursor to cleavage of the bond.

**Keywords:** cluster compounds · density functional calculations · molybdenum · nitrogen fixation

## Introduction

Despite the fact that the molecular structure of the iron–molybdenum cofactor (FeMoco) in nitrogenase has been known for over a decade,[1] a complete understanding of the mechanistic details of dinitrogen reduction remains an elusive goal.[2] Knowledge of the structure of the cofactor, along with the emergence of density functional theory as a quantitative tool for transition-metal systems, has inspired a large number of theoretical studies in this area. The majority of these have focussed on the preferred binding site for molecular nitrogen or its partially reduced derivatives,[3–10] and the relative merits of Mo or Fe in this respect have been hotly debated. Many authors have favoured the iron cluster because of the highly unusual coordinative unsaturation of the iron centres, although a recent higher resolution study of the cofactor, which indicates the presence of a light atom (probably N) at the centre of the cluster,[1c] has raised doubts over this conclusion. The magnetic and spectroscopic properties of the cofactor itself have also been the focus of attention in recent years, most notably in the detailed studies by Noodleman and co-workers into the nature of the magnetic coupling between the high-spin metal ions.[11]

The importance of iron and molybdenum in nitrogen fixation was appreciated long before the structure of the cofactor was known, and the coordination chemistry of nitrogen and its partially reduced derivatives has played a significant role in enhancing our understanding of the process.[12] The chemistry associated with nitrogen reduction is most commonly discussed in the context of the Chatt[13] and Schrock[14] cycles, the key features of which are summarised in Figure 1. The initial steps of the two cycles are similar, involving two ligand-based one-electron reduction steps, ac-

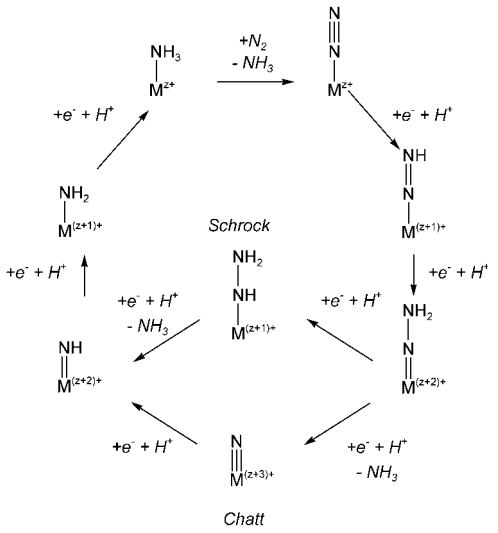


Figure 1. Schematic representation of the Chatt and Schrock cycles for nitrogen reduction.

[a] Dr. J. K. Padden Metzker, Dr. J. E. McGrady
Department of Chemistry, The University of York
Heslington, York, YO10 5DD (UK)
Fax: (+44) 190-443-2516
E-mail: jem15@york.ac.uk

Supporting information for this article is available on the WWW under http://www.chemeurj.org/ or from the author.

 **DOI: 10.1002/chem.200400580**  

companied by a two-electron oxidation of the metal centre, leading to the formation of a hydrazido(2−) (-N-$NH_2$) complex. In the Chatt cycle, the third one-electron reduction step is also ligand-based and is accompanied by a further oxidation of the metal centre, leading to the formation of a nitride. Such high oxidation states are accessible only for electron-rich metal cores[15] such as the zero-valent $M(PR_3)_4$ (M = Mo, W) studied by Chatt and co-workers.[16] In the Schrock cycle, the third one-electron reduction is metal-, rather than ligand-centred, leading to a stable coordinated hydrazide, and the N–N σ bond is only cleaved following the fourth one-electron reduction (possibly via a hydrazine intermediate, $M(NH_2NH_2)$). The key difference in the context of this work is that the metal oxidation state varies by only two units in the Schrock cycle, and hence is more plausible for high-valent metal cores such as $Cp^*MMe_3$ (M = Mo, W). The stoichiometric conversion of $N_2$ to ammonia through both routes is well known,[17] but examples of catalytic ammonia production are rare.[17a,18] Theory has also played a key role in the context of model chemistry, enhancing our understanding of the key electronic requirements for efficient cleavage of the N–N bonds in dinitrogen[19] and its partially reduced derivatives.[20–22]

The polymetallic nature of the FeMoco has encouraged a number of groups to expand the concepts embodied in the Chatt and Schrock cycles into the realm of bimetallic chemistry.[23,24] In a series of recent publications, Talarmin and co-workers have reported the synthesis and electrochemical properties of a number of complexes containing nitrogenous ligands coordinated to a dimolybdenum core, $CpMo^{III}(\mu\text{-}SR)_3Mo^{III}Cp$ (Figure 2).[23] The high metal oxidation states in these systems invite obvious comparison with the Schrock cycle for monometallic species. In the context of nitrogen fixation, the electrochemical reduction of the phenyldiazene species, $[Cp_2Mo_2(\mu\text{-}SMe)_3(\mu\text{-}\eta^1\text{:}\eta^1\text{-}HN{=}NPh)]^+$, is particularly relevant as it yields aniline, along with an ammine ligand, clearly illustrating the capacity of the bimetallic core to support N=N bond cleavage.[23d] Moreover, both reactants and products have been characterised crystallographically, confirming that the structure of the dimolybdenum core $\{CpMo(\mu\text{-}SMe)_3MoCp\}$ is conserved throughout the reaction. The reaction pathway is, however, clearly a complex one with a number of possible intermediates and transition states separating reactants from products. By analogy with the monomeric systems in the Chatt and Shrock cycles, we anticipate that the metal centres may act as a reservoir, providing a source of electrons to facilitate the reductive cleavage of the N=N bond. In this paper, we use density functional theory to probe the intimate electronic role of the bimetallic core in the reaction, paying particular attention to the transfer of electrons between metal and ligand.

## Results and Discussion

**Geometric structure of $[Cp_2Mo_2(\mu\text{-}SMe)_3(\mu\text{-}\eta^1\text{:}\eta^1\text{-}HN{=}NPh)]^+$**: The fully characterised structure of $[Cp_2Mo_2(\mu\text{-}SMe)_3(\mu\text{-}\eta^1\text{:}\eta^1\text{-}HN{=}NPh)]^+$ [23a] provides an opportunity to benchmark the chosen theoretical model, and also to examine the extent to which simplifying the system affects the geometry. $[Cp_2Mo_2(\mu\text{-}SMe)_3(\mu\text{-}\eta^1\text{:}\eta^1\text{-}HN{=}NPh)]^+$ has been isolated in two distinct conformers, *syn* and *anti*, differing only in the relative orientation of the methyl groups on the bridging ligands *cis* to the coordinated diazene. In the *syn* conformer, both methyl groups are directed towards the diazene, while in the *anti* form they are oriented in opposite directions. Of the two, only the *syn* conformer has been structurally characterized, while the closely related species $[Cp_2Mo_2(\mu\text{-}SMe)_3(\mu\text{-}NH_2)]$ crystallizes in the *anti* conformation. For both model systems, $[Cp_2Mo_2(\mu\text{-}SH)_3(\mu\text{-}\eta^1\text{:}\eta^1\text{-}HN{=}NH)]^+$ and $[Cp_2Mo_2(\mu\text{-}SH)_3(\mu\text{-}NH_2)]$, the conformation of the bridging ligands is found to have negligible impact on the optimized structural parameters of the core. Moreover, calculated energy differences between the *syn* and *anti* isomers are uniformly small ($< 0.5\ kcal\,mol^{-1}$), with the latter the more stable. In light of the minor structural and energetic differences between the two conformers, we consider only the more stable *anti* isomer (shown in Figure 2) in this work.

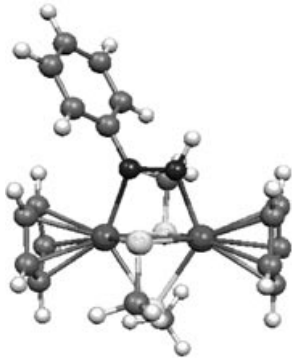

Figure 2. Molecular structure of $[Cp_2Mo_2(\mu\text{-}SMe)_3(\mu\text{-}\eta^1\text{:}\eta^1\text{-}HN{=}NPh)]^+$.

The optimised structure of $[Cp_2Mo_2(\mu\text{-}SMe)_3(\mu\text{-}\eta^2\text{-}HN{=}NPh)]^+$ is shown in Figure 2 and pertinent structural parameters calculated using the gradient corrected BP86 functional are compared to the available experimental structural data in Table 1. All calculated bond lengths are overestimated relative to experiment, the most significant discrepancies being in the Mo–Mo and Mo–N bond lengths, where calculated values are in error by 0.07 Å. Errors of this magnitude are, however, typical of singly bonded bimetallic species,

Table 1. Optimised structural parameters for $[Cp_2Mo_2(\mu\text{-}SR)_3(\mu\text{-}\eta^1\text{:}\eta^1\text{-}HN{=}NR')]^+$. All distances in Å.

| | R = Me, R′ = Ph | | R = H, R′ = Ph | R = H, R′ = H |
|---|---|---|---|---|
| | X-ray[a][23] | BP86 | BP86 | BP86 |
| Mo–Mo | 2.650(2) | 2.72 | 2.72 | 2.72 |
| Mo–$N_{R'}$ | 2.137(8) | 2.19 | 2.19 | 2.11 |
| Mo–$N_H$ | 2.018(9) | 2.09 | 2.09 | 2.11 |
| N–N | 1.324(11) | 1.31 | 1.30 | 1.30 |
| Mo–$S_{cis}$ | 2.44 | 2.53 | 2.53 | 2.53 |
| Mo–$S_{trans}$ | 2.47 | 2.53 | 2.53 | 2.55 |

particularly where counterions are present to perturb the solid-state structure. The removal of the methyl substituents (R = H, R′ = Ph) causes only small changes (0.02 Å) in the metal core, while further removal of the phenyl group (R = R′ = H) causes a 0.08 Å decrease in the Mo–N bond length. Overall, however, the data collected in Table 1 suggest that the simplest system, $[Cp_2Mo_2(\mu\text{-}SH)_3(\mu\text{-}\eta^1\text{:}\eta^1\text{-}HN{=}NH)]^+$, (Figure 3a) provides an adequate representation of the parent complex, and so this computationally expedient model (abbreviated as **1**:**1**$^+$) will be used to explore the reduction pathway.

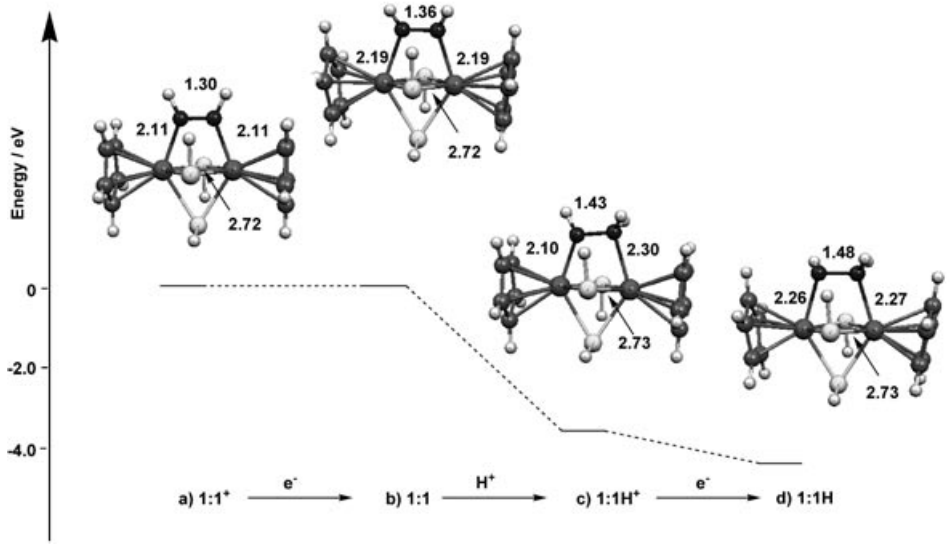


Figure 3. Optimised structures of minima involved in the initial ECE reaction (reduction of the π component of the N=N bond). The gas-phase electron affinities for the reduction steps are reported relative to that for **1**:**1**$^+$ ($\Delta E = -4.89$ eV) (see text). The energy of the protonation step is reported relative to the process $H_2O + H^+ \rightarrow H_3O^+$.

**Ground-state electronic structure of $[Cp_2Mo_2(\mu\text{-}SH)_3(\mu\text{-}\eta^1\text{:}\eta^1\text{-}HN{=}NH)]^+$ (1:1$^+$)**: The three highest occupied molecular orbitals of **1**:**1**$^+$ (Figure 4a) have Mo–Mo σ, δ* and δ symmetry, consistent with the formal Mo–Mo bond order of one proposed by Schollhammer et al. based on electron count.[23a] This simplified description, however, obscures a number of significant details that impact on the electrochemical behaviour. In particular, the Mo–Mo δ* orbital is strongly mixed with the out-of-plane N=N π*, as a result of which the bonding combination (**46a**, 69% Mo–Mo δ*, 31% N=N π*) is significantly stabilized. The antibonding combination forms the LUMO of the complex (**48a**), and the mixing of ligand and metal orbitals (43% Mo–Mo δ* 57% N=N π*) suggests that the initial reduction process will be strongly delocalised over both metal and ligand. In contrast, the HOMO (**47a**, Mo–Mo δ) is completely localized on the metal centres and is essentially non-bonding. This orbital has the potential, therefore, to act as an electronic "buffer", supplying electrons to the ligand without significantly disrupting the structure of the metal core. The Mo–Mo σ orbital (**45a**), is, in contrast, strongly bonding and therefore unlikely to participate in any redox-based chemistry. Instead, it plays a key role in maintaining the structural integrity of the core throughout the reaction.

Before going on to consider the structural and electronic consequences of the reduction process, it is important to emphasise that the N=N double bond in diazene has two distinct components, σ and π, and reductive cleavage of *both* is required to achieve the release of ammonia. In the following discussion, we will discuss each of these two steps in turn, and argue that the fundamentally different orientation of the two redox-active orbitals (N–N π* and σ*) dictates the complex structural reorganisation involved in the reduction pathway.

**Reduction in the absence of acid**: Electrolysis of the cationic diazene complex, $[Cp_2Mo_2(\mu\text{-}SMe)_3(\mu\text{-}\eta^2\text{-}HN{=}NPh)]^+$, at −1.8 V has been shown to yield the neutral species $[Cp_2Mo_2(\mu\text{-}SMe)_3(\mu\text{-}\eta^1\text{:}\eta^1\text{-}N{=}NPh)]$.[23c,d] The structure of the model species, $[Cp_2Mo_2(\mu\text{-}SH)_3(\mu\text{-}\eta^1\text{:}\eta^1\text{-}HN{=}NH)]$ (**1**:**1**) arising from a one-electron transfer to **1**:**1**$^+$, was optimized starting from the geometry of the cationic parent (Figure 3b). The additional electron causes a significant elongation of both N–N (0.06 Å) and Mo–N (0.08 Å) bonds, consistent with the antibonding character of the SOMO shown in Figure 4b, and the two substituents on the diazene unit bend out of the Mo-N-N-Mo plane. The net spin densities of 0.39 and 0.10 on the nitrogen and molybdenum centres, respectively, confirm that this initial reduction is largely ligand-, rather than metal-centred. The reduced product, **1**:**1**, is unstable with respect to loss of $^1/_2H_2$ and formation of $[Cp_2Mo_2(\mu\text{-}SH)_3(\mu\text{-}\eta^2\text{-}N{=}NH)]$ ($\Delta E = -0.4$ eV). Thus, our calculations are in agreement with experiment; in the absence of acid, the thermodynamically favoured outcome is the reductive generation of hydrogen, rather than cleavage of the N–N bond.[23d]

**Reduction in the presence of acid**: Before describing the reduction process in detail, we wish to comment on our interpretation of the calculated electron affinities and protonation energies. The absolute values of these two quantities cannot be compared directly to experimental electrode potentials and basicities because they take as their reference point the energies of isolated gas-phase electrons and protons, clearly poor models for the electrode and solvated proton, respectively. The calculated electron affinities can, however, be used in a relative sense to assess the driving force of successive reduction steps. Thus, if the calculated electron affinity of the starting material, **1**:**1**$^+$, ($\Delta E = -4.89$ eV) is taken as an internal standard, any intermediate

  

with a more exothermic electron affinity (i.e., $\Delta E < -4.89$ eV) should also be spontaneously reduced at the same potential. An important corollary of this interpretation is that any such intermediate is unlikely to be isolated under electrolysis conditions. In all subsequent sections, the electron affinity for a given intermediate, **I**, is therefore reported *relative* to that of **1**:**1**$^+$ (i.e., the calculated energy for the process **I**$^+$ + **1**:**1**→**I** + **1**:**1**$^+$). In this way, negative values imply that the intermediate in question should be spontaneously reduced at the potential required to reduce **1**:**1**$^+$. Similarly, the reported protonation energies are referenced to the gas-phase protonation energy of water (i.e., the calculated energy for the process **I** + $H_3O^+$→**I**$H^+$ + $H_2O$).

In the presence of excess acid, the reduction of **1**:**1**$^+$ leads to cleavage of the N–N bond rather than generation of $H_2$.[23c,d] Although no intermediates have been isolated, the accumulated experimental evidence suggests that the complete process can be divided into two distinct phases, an initial two-electron-one-proton (ECE) step, separated from the remaining reduction and protonation steps by a slow chemical step. In the following sections, each of these processes is considered separately.

**First ECE step—Reduction of the π component of the N–N bond**: The observed irreversibility of the electrode process clearly indicates that the primary reduction product (**1**:**1**) is protonated in acidic conditions. Three possible sites for this protonation have been of considered (nitrogen and two distinct sulphurs) and, consistent with earlier extended Hückel calculations,[23i] the nitrogen sites were found to be the most basic. The optimised structure of the reduced and protonated product, **1**:**1H**$^+$, is shown in Figure 3c, where the N–N bond length of 1.43 Å is characteristic of a single, rather than double, N–N bond, and the Mo–N bonds are highly asymmetric (2.30 and 2.10 Å). The dramatic structural changes induced by the protonation are indicative of a substantial redistribution of charge in the molecule. Protonation at the nitrogen centre introduces N–H σ character into the N–N π* orbital, strongly stabilizing it relative to the metal-based manifold (Figure 4b,c). As a result, a single electron is transferred from the Mo–Mo δ orbital (HOMO of **1**:**1**$^+$) into N–N π*, leaving a vacancy in the former. In formal terms, the diazene ligand has been reduced to the hydrazido(1−) level ($NH_2$-$NH^-$), while the metal core has been oxidised to $Mo^{III}Mo^{IV}$. Significant charge redistribution has also been noted by Tuczek and co-workers upon protonation of coordinated $N_2$.[21c] The oxidation of the core is strongly localised at a single $Mo^{IV}$ centre, which can be effectively stabilised by π donation from the negatively charged pole of the hydrazido ligand (orbital **48a** of **1**:**1H**$^+$), leading to the marked asymmetry in the Mo–N distances. The calculations therefore indicate that a combination of *one-electron reduction* and protonation of the complex **1**:**1**$^+$ results in the the *two-electron reduction* of the diazene unit (to $NH_2NH^-$) with concomitant *one-electron oxidation* of the molybdenum core (to $Mo^{III}Mo^{IV}$).

As a result of the redistribution of charge induced by the protonation, the second electron transfer step in the ECE mechanism, leading to **1**:**1H**, is metal- ($Mo^{IV}$ to $Mo^{III}$) rather than ligand-centred. It is unsurprising, then, that the calculated electron affinity of **1**:**1H**$^+$ is greater than that of **1**:**1**$^+$ (−5.71 vs −4.89 eV), and therefore that **1**:**1H**$^+$ has not been isolated as an intermediate. The reduction of **1**:**1H**$^+$ also eliminates the π-donation pathway from the hydrazido(1−) ligand to the metal, as a result of which the Mo–N bond lengths are equalized, and the increased electron repulsions within the $NH_2$-$NH^-$ ligand cause a further elongation of the N–N bond (Figure 3d). In terms of the role of the metal core, it is significant that the Mo-Mo separation varies by less than 0.02 Å across the series **1**:**1**$^+$→**1**:**1**→**1**:**1H**$^+$→**1**:**1H**, despite the extensive electronic redistribution described above. This rigidity can ultimately be traced to the non-bonding nature of the redox-active metal-based orbital (Mo–Mo δ), which has little impact on the structure. The σ bonding orbital, in contrast, remains unperturbed throughout the process and retains the integrity of the core throughout the redox cycle (Figure 4a–c).

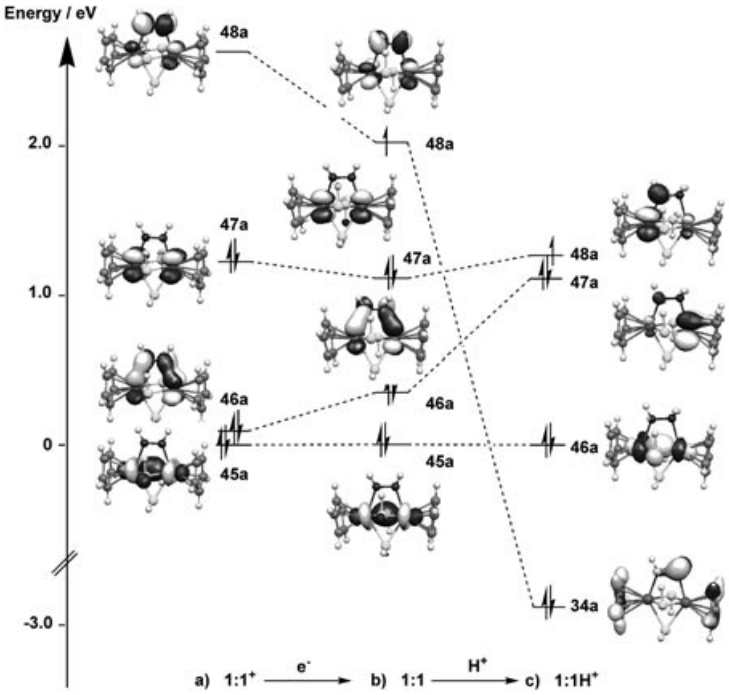


Figure 4. Evolution of the frontier orbitals in the reductive cleavage of the π component of the N=N bond (**1**:**1**$^+$→**1**:**1**→**1**:**1H**$^+$). The Mo–Mo σ orbital is taken as the energetic reference point.

**Subsequent reduction steps—Reduction of the σ component of the N–N bond**: The electrochemical data indicate that the initial ECE step, leading to **1**:**1H**, is separated from further reduction by a slow chemical step, which Le Grand et al. have proposed to be a rearrangement from $\eta^1$:$\eta^1$- to $\eta^1$-coordination of the ligand.[23d] The optimised structures of the $\eta^1$:$\eta^1$- and $\eta^1$-coordinated isomers (**1**:**1H** and **1H**) are compared in Figure 5a and c. The switch in coordination mode induces a contraction in the Mo–Mo and Mo–N bonds (0.12 and 0.07 Å, respectively), but the N–N bond length is marginally shorter in **1H**, indicating that the isomerisation does not in itself induce cleavage of the bond.

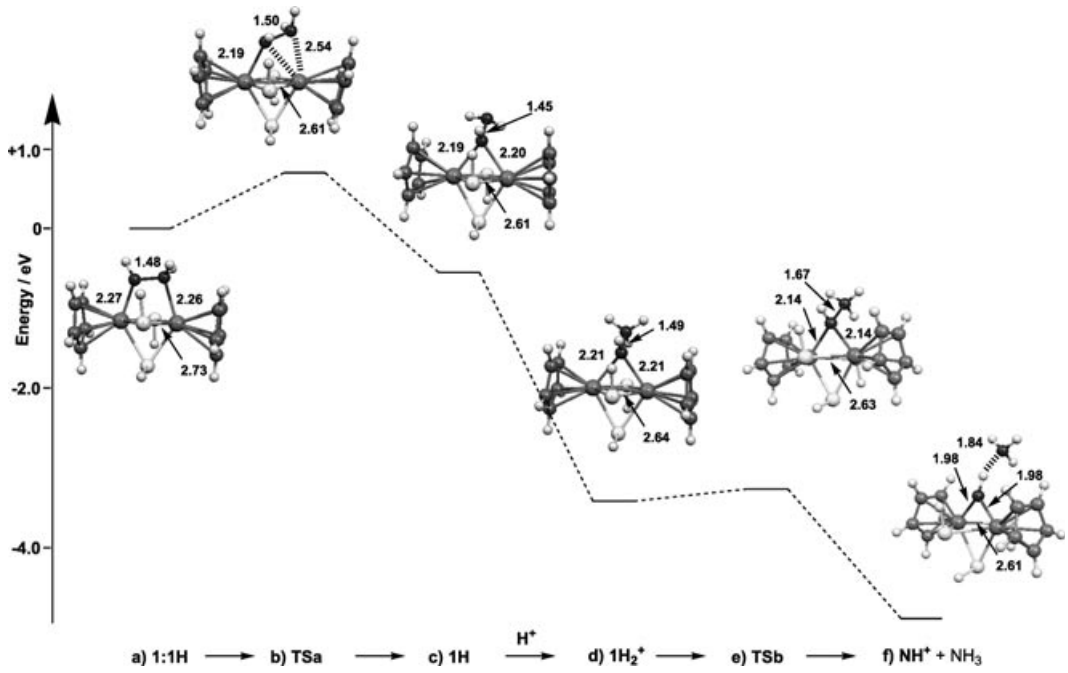


Figure 5. Optimised structures of minima involved in the reduction of the σ component of the N=N bond. The protonation energy is reported relative to the process $H_2O + H^+ \rightarrow H_3O^+$.

The driving force for the $\eta^1{:}\eta^1 \rightarrow \eta^1$ isomerisation ($\Delta E = -0.57$ eV) is provided by the preference of the negative pole of the hydrazido(1−) ligand to occupy a bridging position between the two $Mo^{III}$ centres rather than binding to only one. In contrast, the corresponding $\eta^1{:}\eta \rightarrow \eta^1$ rearrangement is strongly endothermic at the previous step in the cycle (**1**:**1H**$^+ \rightarrow$**1H**$^+$) because, as noted previously, the $\eta^1{:}\eta^1$-mode allows the negatively charged pole of the hydrazido(1−) ligand to bond exclusively to the localised $Mo^{IV}$ centre. A transition state, **TSa**, connecting the $\eta^1{:}\eta^1$ and $\eta^1$ isomers has been located (Figure 5b), where the $N_2$ unit is tilted such that the negatively charged pole migrates towards the opposite metal centre. The transition state lies 0.77 eV above **1**:**1H**, a barrier that is fully consistent with the proposal that this step is rate limiting.

Having established that the $\eta^1{:}\eta^1 \rightarrow \eta^1$ isomerisation is both thermodynamically favourable and kinetically feasible at the doubly reduced, singly protonated level, we examine the structural and electronic consequences of further reduction on the $\eta^1$ surface. Protonation of **1H** gives the cationic product, **1H**$_2^+$ (Figure 5d), where the N−N bond (1.49 Å) is marginally elongated relative to **1H**, but the structure is otherwise affected to only a minor extent. **1H**$_2^+$, however, lies in a very shallow local minimum on the potential energy surface, and is unstable with respect to cleavage of the N−N σ bond with formation of $[Cp_2Mo_2(\mu\text{-}SH)_3(\mu\text{-}NH)]^+$, denoted **NH**$^+$, and $NH_3$. Following cleavage of the N−N bond, the ammonia molecule remains hydrogen bonded to amide ligand (Figure 5f). The low barrier (**TSb**, Figure 5e, lies only 0.07 eV above **1H**$_2^+$) suggests that N−N bond cleavage will not be rate limiting.

The redistribution of electron density associated with the **1H**$\rightarrow$**1H**$_2^+ \rightarrow$**NH**$^+$ + $NH_3$ processes is summarised in Figure 6. Protonation of **1H** introduces N–H σ character into the N–N σ* orbital, and elongation of the N−N bond causes this orbital to fall below the near degenerate Mo–Mo δ/δ* pair (**47a**, **48a**) orbital. A transfer of two electrons from metal to ligand then results in cleavage of the bond, with concomitant oxidation of the metal core to the $Mo^{IV}Mo^{IV}$ level, which is again strongly stabilised by π donation from the bridging imido ligand. The redistribution of electron density involved in the cleavage of the σ component of the N−N bond is, in fact, remarkably similar in qualitative terms to that described previously for the π bond, where protonation of **1**:**1** induced electron transfer (in this case a single electron) from the Mo–Mo δ orbital into the partially occupied ligand π* orbital. The central role of the Mo–Mo δ orbital as a source of electrons in both processes also explains the need for the $\eta^1{:}\eta^1 \rightarrow \eta^1$ rearrangement prior to cleavage of the σ component of the N−N bond. In the absence of such a rearrangement, protonation of **1**:**1H** yields the cationic species **1**:**1H**$_2^+$, a hydrazine complex. By analogy to the isoelectronic species **1H**$_2^+$, N−N bond cleavage in **1**:**1H**$_2^+$ could, in principle, lead to formation of a $Mo^{IV}Mo^{IV}$ core, each metal centre being stabilised by a terminal $NH_2$ ligand (Figure 7). We have, however, been unable to locate a transition state for this process, or even a minimum corresponding to the structure with a cleaved N−N bond. The dramatic differences between the $\eta^1{:}\eta^1$- and $\eta^1$-potential energy surfaces can traced to the overlap of the frontier orbitals, shown schematically in Figure 7. In the $\eta^1$-mode (**1H**$_2^+$) there is significant overlap between the Mo–Mo δ and N–N σ* orbitals, as a result of which the two orbitals mix along the reaction coordinate. An avoided crossing then affords smooth transfer of electron density from the metal to the ligand. In the $\eta^1{:}\eta^1$ mode, however, the Mo–Mo δ and

  

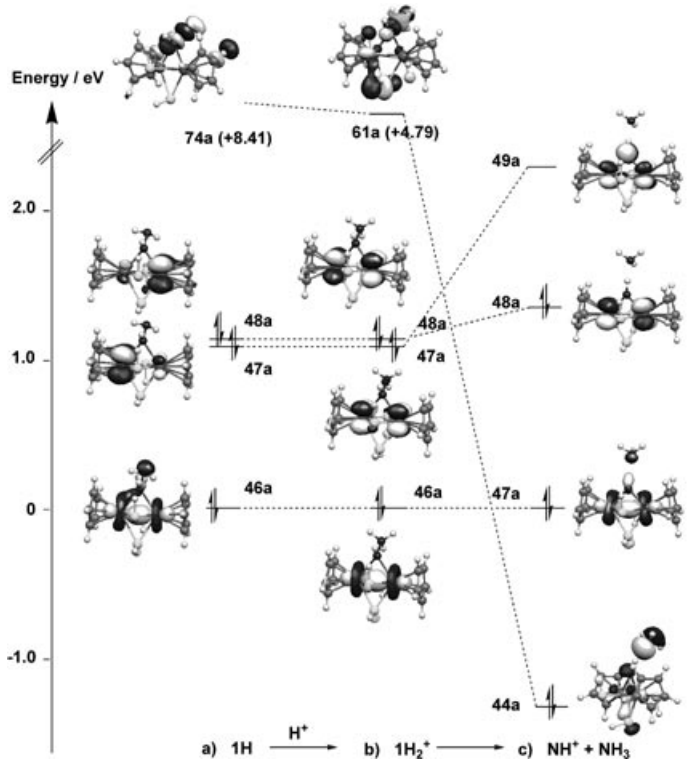


Figure 6. Evolution of the frontier orbitals in the reductive cleavage of the σ component of the N=N bond (**1H**→**1H$_2^+$**→**NH$^+$** + $NH_3$). The Mo–Mo σ orbital is taken as the energetic reference point. Numbers in parentheses indicate energies of high-lying orbitals.

N–N σ* orbitals are orthogonal, and so electron transfer is formally forbidden. A similar situation was noted by Tuczek and co-workers in their recent study of the $Mo^{IV}$ species, $[MoF(PH_3)_4(N\text{-}NH_3)]^{2+}$, where the orthogonality of the doubly occupied Mo $d_{xy}$ orbital and N–N σ* leads to an estimated activation barrier in excess of 40 kcalmol$^{-1}$ (~1.7 eV).[21d] The lack of overlap in the bimetallic system could, in principle, be alleviated by twisting the hydrazine ligand relative to the Mo–Mo axis, but only at the expense of weakening the Mo–N bonds. The net result is that concerted transfer of two electrons from the metal core to the σ* orbital is symmetry forbidden on the $\eta^1$:$\eta^1$-surface, leaving the $\eta^1$:$\eta^1$→$\eta^1$ rearrangement as the only energetically accessible pathway. This analysis clearly illustrates the crucial role of the Mo–Mo δ orbital as an electron source: in circumstances where the ligand cannot access this electron density for symmetry reasons, cleavage of the N–N bond is effectively blocked.

**Regeneration of $Mo^{III}Mo^{III}$ core—Reduction of $[Cp_2Mo_2(\mu\text{-}SH)_3(\mu\text{-}NH)]^+$**: The reductive electrochemistry of the metal-based product remaining following N–N bond cleavage, $[Cp_2Mo_2(\mu\text{-}SMe)_3(\mu\text{-}NH)]^+$ has been the subject of a detailed experimental study.[23g] In this section, we use theory to shed light on some of the unusual observations reported in that paper. Reduction of $[Cp_2Mo_2(\mu\text{-}SH)_3(\mu\text{-}NH)]^+$ (abbreviated as **NH$^+$**) to **NH** results in a 0.09 Å elongation of the Mo–N bonds and a significant pyramidalisation at the nitrogen centre, and the net spin densities of 0.29 (Mo) and 0.36 (N) confirm that the SOMO is strongly delocalised over the whole Mo-N-Mo skeleton. The high spin density at the nitrogen atom is fully consistent with the ability of **NH** to abstract a hydrogen atom from solvent.[23g] In the context of the overall reduction of the diazene complex, **1**:**1$^+$**, it is significant that the gas-phase electron affinity of **NH$^+$** is 0.71 eV more negative than that of **1**:**1$^+$**, again consistent with the fact that it has not been possible to isolate it as an intermediate.

Whilst a potential of −1.25 V is required to reduce $[Cp_2Mo_2(\mu\text{-}SMe)_3(\mu\text{-}NH)]^+$, reoxidation of a daughter product was observed at a significantly more positive potential, −0.65 V. Talarmin and co-workers have rationalised this result by proposing that the oxidation of the pyramidalised imide, **NH**, produces a second isomer of **NH$^+$**, also with a pyramidal nitrogen, rather than the planar structure shown in Figure 8a.[23g] A survey of the singlet potential energy surface has failed to reveal any low-lying minima other than the **NH$^+$**, but a low-lying triplet state, **$^3$NH$^+$**, has been located, with a pyramidal nitrogen and significant unpaired spin density on both metal (0.89) and nitrogen (0.33). The calculated singlet–triplet gap of 0.76 eV is of the same magnitude as the separation between the two redox processes (0.6 V). Moreover, the calculated electron affinity of **$^3$NH$^+$** is very similar to that of the protonated species, **$NH_2^+$** (see below), which exhibits a reversible reduction at very similar potential to the daughter product (−0.64 V). Thus the formation of a metastable triplet state, **$^3$NH$^+$**, with a bent imide unit, provides an explanation for the observed electrochemical

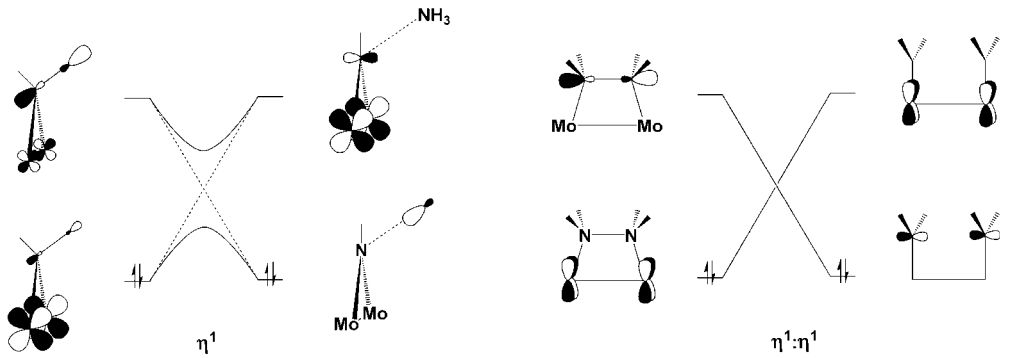


Figure 7. Schematic comparison of electron transfer pathways for N–N σ bond cleavage in the $\eta^1$- and $\eta^1$:$\eta^1$-coordination modes.

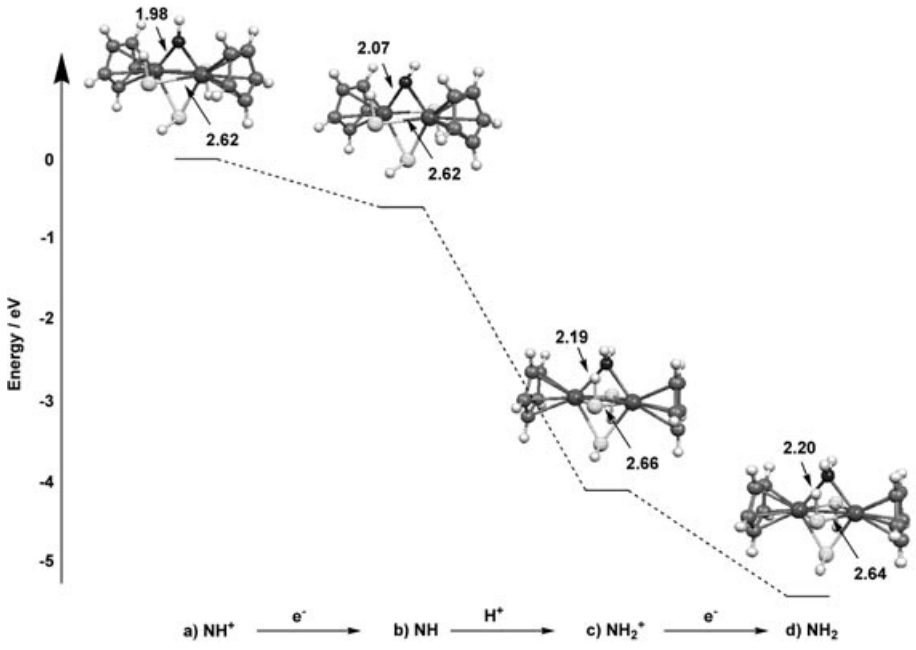


Figure 8. Optimised structures of minima involved in the regeneration of the $Mo^{III}Mo^{III}$ core. The gas-phase electron affinities for the reduction steps are reported relative to that for **1**:**1**$^+$ ($\Delta E = -4.89$ eV) (see text). The protonation energy is reported relative to the process $H_2O + H^+ \rightarrow H_2O$.

behaviour. In the presence of acid, **NH** is protonated to form an amide species $[Cp_2Mo_2(\mu\text{-}SH)_3(\mu\text{-}NH_2)]^+$ (**NH$_2$**$^+$). This protonation step strongly stabilises the final nitrogen-based lone pair, effectively eliminating any π donation into the vacancy in the $Mo^{III}Mo^{IV}$ core. As a result, the Mo–N bonds are further elongated, and the unpaired electron density resides in an orbital with almost exclusively metal character [net spin densities: 0.50 (Mo), −0.02 (N)]. The final reduction step, leading to $[Cp_2Mo_2(\mu\text{-}SH)_3(\mu\text{-}NH_2)]$ (**NH$_2$**) is therefore entirely metal based, and regenerates the $Mo^{III}Mo^{III}$ core. The absence of π donation in **NH$_2$**$^+$ results in a very high electron affinity, 1.41 eV more negative than that of **1**:**1**$^+$, confirming that the final reduction process will again be spontaneous at the potential required to induce reduction of the starting material.

## Summary

The calculations reported herein indicate that the bimetallic core plays a key role in mediating the reductive cleavage of the N≡N bond by providing a source of high-energy electrons. External reduction and protonation induces electron transfer from the δ orbital to the ligand, and the resulting vacancy in the metal core is stabilized by π donation from the reduced ligand. In this way, the redox process is effectively delocalised over the entire $Mo_2N_2$ skeleton, reducing the barriers for consecutive electron transfers. A close examination of the electronic structure reveals that the highest energy electrons (and therefore those most accessible to the substrate) are located in the Mo–Mo δ orbital, and the symmetry of this orbital plays a key role in determining the course of the reduction process. The reductive cleavage of the π and σ components of the N=N double bond in diazene are fundamentally distinct processes, each requiring a specific orientation of the N–N unit relative to the metal core to allow efficient electron transfer from the Mo–Mo δ orbital to the ligand. The $\eta^1$:$\eta^1$-coordination mode provides optimal overlap between the N–N π* and Mo–Mo δ orbitals, and so the first ECE step occurs without rearrangement. In the same $\eta^1$:$\eta^1$-coordination geometry, however, the N–N σ* orbital is orthogonal to Mo–Mo δ, effectively blocking the cleavage of the σ component of the bond. Isomerisation to the $\eta^1$-coordination mode reinstates the all-important overlap between the metal- and ligand-based orbitals, and is therefore a necessary precursor to cleavage of the N–N bond. It is interesting to speculate that the complex structure of the FeMoco may allow similar changes in coordination mode to occur during the reduction of the N≡N triple bond.

The key steps in the reduction cycle are collected in Figure 9. Of the four reduction processes, only the first, **1**:**1**$^+$ →**1**:**1**, is significantly localised on the ligand itself. The next two, **1**:**1H**$^+$→**1**:**1H** and **NH**$^+$→**NH**, are essentially $Mo^{IV} \rightarrow Mo^{III}$ processes, although the oxidised metal centre is strongly stabilised by π donation from a nitrogen-based lone pair in each case. The final reduction process (**NH$_2$**$^+$→**NH$_2$**) is almost completely metal-centred ($Mo^{IV} \rightarrow Mo^{III}$) as the bridging amide ligand is unable to stabilise the oxidised metal centre through π donation. The increasing metal character of the successive reduction events is reflected in progressively more exothermic electron affinities, ensuring that the initial electron transfer to $[Cp_2Mo_2(\mu\text{-}SMe)_3(\mu\text{-}\eta^2\text{-}HN{=}NPh)]^+$ induces a cascade leading, ultimately, to complete reduction of the nitrogenous ligand in acidic media.

## Computational Methods

Calculations were performed using the Amsterdam Density Functional (ADF) package, version 2002.01.[25] A triple-ζ + polarisation Slater-type basis was employed for molybdenum and a double-ζ + polarisation basis for carbon, nitrogen, sulphur and hydrogen. All core electrons (1s–3p for Mo, 1s–2p for S and 1 s for C, N) were frozen. Calculations were performed using the local density approximation,[26] in conjunction with the gradient corrections to exchange (Becke)[27] and correlation (Perdew).[28] Structures of transition states were initially optimised using the Gaussian98 package[29] with the same functional and the LANL2DZ basis[30] on all atoms, and characterised by the presence of a single imaginary frequency. The optimised coordinates were then used as starting geometries for an ADF calculation, where the transition state was characterized by a single negative eigenvalue in the Hessian matrix.

  

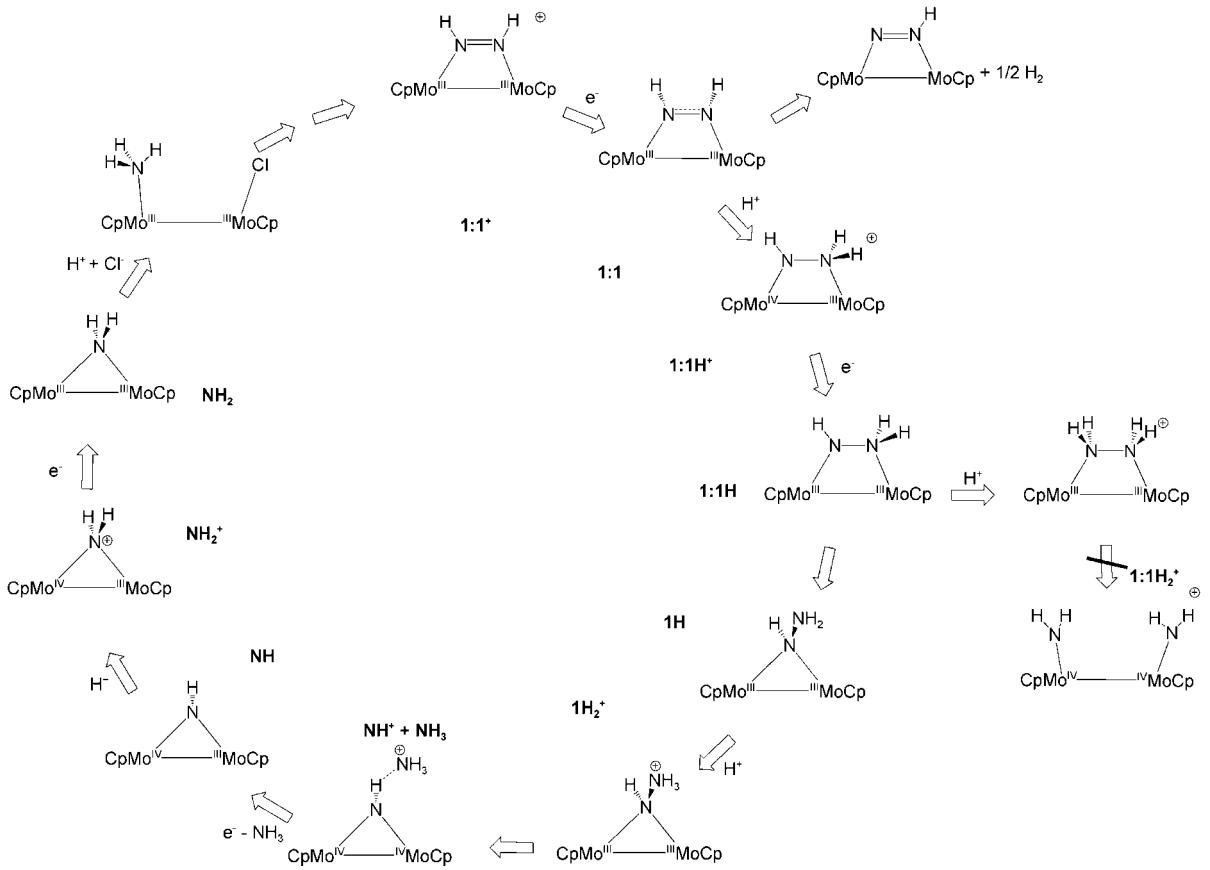


Figure 9. Summary of reaction profile for the reductive cleavage of the N=N bond.

## Acknowledgement

This work was supported by funding from the BBSRC.

[1] a) J. Kim, D. C. Rees, *Nature* **1992**, *360*, 553; b) J. Kim, D. C. Rees, *Science* **1992**, *257*, 1677; c) O. Einsle, I. A. Tezcan, S. L. A Andrade, B. Schmid, M. Yoshida, J. B. Howard, D. C. Rees, *Science* **2002**, *297*, 1696.

[2] a) B. K. Burgess, D. J. Lowe, *Chem. Rev.* **1996**, *96*, 2983; b) R. R. Eady, *Chem. Rev.* **1996**, *96*, 3013.

[3] H. Deng, R. Hoffmann, *Angew. Chem.* **1993**, *105*, 1125; *Angew. Chem. Int. Ed. Engl.* **1993**, *32*, 1062.

[4] a) I. G. Dance, *Aust. J. Chem.* **1994**, *47*, 979; b) I. G. Dance, *Chem. Commun.* **1997**, 165; c) I. G. Dance, *Chem. Commun.* **1998**, 523; d) I. G. Dance, *Chem. Commun.* **2003**, 324.

[5] a) M. C. Durrant, *Biochemistry* **2002**, *41*, 13934; b) M. C. Durrant, *Biochemistry* **2002**, *41*, 13946; c) M. C. Durrant, *Inorg. Chem. Commun.* **2001**, *4*, 60; d) M. C. Durrant, *Biochem. J. 2001, 355*, 569.

[6] a) K. K. Stavrev, M. C. Zerner, *Chem. Eur. J.* **1996**, *2*, 83; b) K. K. Stavrev, M. C. Zerner, *Theor. Chim. Acta* **1997**, *96*, 141; c) K. K. Stavrev, M. C. Zerner, *Int. J. Quantum Chem.* **1998**, *70*, 1159.

[7] a) P. E. M. Siegbahn, J. Westerberg, M. Svensson, R. H. Crabtree, *J. Phys. Chem. B* **1998**, *102*, 1615; b) P. E. M. Siegbahn, M. R. A. Blomberg, *Chem. Rev.* **2000**, *100*, 421.

[8] a) T. H. Rod, J. K. Nørskov, *J. Am. Chem. Soc.* **2000**, *122*, 12751; b) T. H. Rod, B. Hammer, *Phys. Rev. Lett.* **1999**, *82*, 4054; c) T. H. Rod, A. Logadottir, J. K. Nørskov, *J. Chem. Phys.* **2000**, *112*, 5343; d) B. Hinneman, J. K. Nørskov, *J. Am. Chem. Soc.* **2003**, *125*, 1466; e) B. Hinneman, J. K. Nørskov, *Phys. Chem. Chem. Phys.* **2004**, *6*, 843.

[9] a) R. K. Szilagyi, D. G. Musaev, K. Morokuma, *Inorg. Chem.* **2001**, *40*, 766; b) R. K. Szilagyi, D. G. Musaev, K. Morokuma, *J. Mol. Struct.* **2000**, *506*, 131.

[10] a) U. Huniar, R. Ahlrichs, D. Coucouvanis, *J. Am. Chem. Soc.* **2004**, *126*, 2588; b) V. Vrajmasu, E. Münck, E. L. Bominaar, *Inorg. Chem.* **2003**, *42*, 5974.

[11] a) T. Lovell, J. Li, T. Liu, D. A. Case, L. Noodleman, *J. Am. Chem. Soc.* **2001**, *123*, 12392; b) T. Lovell, J. Li, D. A. Case, L. Noodleman, *J. Am. Chem. Soc.* **2003**, *125*, 8377; c) T. Lovell, J. Li, D. A. Case, L. Noodleman, *J. Am. Chem. Soc.* **2002**, *124*, 4546; d) T. Lovell, R. A. Torres, W.-G. Han, T. Liu, D. A. Case, L. Noodleman, *Inorg. Chem.* **2002**, *41*, 5744; e) T. Lovell, J. Li, D. A. Case, L. Noodleman, *J. Biol. Inorg. Chem.* **2002**, *7*, 735; f) L. Noodleman, T. Lovell, W.-G. Han, J. Li, F. Himo, *Chem. Rev.* **2004**, *104*, 459.

[12] a) R. N. F. Thornley, D. J. Lowe, in Molybdenum Enzymes (Ed. T. G. Spiro), Wiley, New York, **1985**; b) F. Barriere, *Coord. Chem. Rev.* **2003**, *236*, 71; c) B. A. MacKay, M. D. Fryzuk, *Chem. Rev.* **2004**, *104*, 385; d) M. D. Fryzuk, S. A. Johnson, *Coord. Chem. Rev.* **2000**, *200*, 379; e) S. C. Lee, R. H. Holm, *Chem. Rev.* **2004**, *104*, 1135. f) M. Hidai, *Coord. Chem. Rev.*, **1999**, *185*, 99; g) G. J. Leigh, *Acc. Chem. Res.* **1992**, *25*, 177; h) T. A. Bazhenova, A. E. Shilov, *Coord. Chem. Rev.* **1995**, *144*, 69; i) C. M. Kozak, P. Mountford, *Angew. Chem.* **2004**, *116*, 1206; *Angew. Chem. Int. Ed.* **2004**, *43*, 1886.

[13] a) R. A. Henderson, G. J. Leigh, C. J. Pickett, *Adv. Inorg. Chem. Radiochem.* **1983**, *27*, 197; b) C. J. Pickett, *J. Biol. Inorg. Chem.* **1996**, *1*, 601; c) R. L. Richards, *Coord. Chem. Rev.* **1996**, *154*, 83; d) J. Chatt, A. J. Pearman, R. L. Richards, *J. Chem. Soc. Dalton Trans.* **1977**, 1852.

[14] a) R. R. Schrock, T. E. Glassman, M. G. Vale, M. Kol, *J. Am. Chem. Soc.* **1993**, *115*, 1760; b) R. R. Shrock, *Pure Appl. Chem.* **1997**, *69*, 2197.

[15] a) C. E. Laplaza, C. C. Cummins, *Science* **1995**, *268*, 861; b) C. E. Laplaza, M. J. A. Johnson, J. C. Peters, A. L. Odom, E. Kim, C. C.

  

Cummins, G. N. George, I. J. Pickering, *J. Am. Chem. Soc.* **1996**, *118*, 8623; c) A. Caselli, E. Solari, R. Scopelliti, C. Floriani, N. Re, C. Rizzoli, A. Chiesi-Villa, *J. Am. Chem. Soc.* **2000**, *122*, 3652.
[16] J. Chatt, J. A. Pearman, R. L. Richards, *Nature* **1975**, *253*, 39.
[17] a) C. J. Pickett, J. Talarmin, *Nature* **1985**, *317*, 652; b) M. Hidai, Y. Mizobe, *Chem. Rev.* **1995**, *95*, 1115.
[18] a) R. R. Schrock, D. Yandulov, *Science* **2003**, *301*, 76; b) R. R. Schrock, *Chem. Commun.* **2003**, 2389.
[19] a) Q. Cui, D. G. Musaev, M. Svensson, S. Sieber, K. Morokuma, *J. Am. Chem. Soc.* **1995**, *117*, 12366; b) D. V. Khoroshun, D. G. Musaev, K. Morokuma, *Organometallics* **1999**, *18*, 5653; c) V. M. E. Bates, G. K. B. Clentsmith, F. G. N. Cloke, J. C. Green, H. D. L. Jenkin, *Chem. Commun.* **2000**, 927; d) J. Hahn, C. R. Landis, V. A. Nasluzov, K. M. Neyman, N. Rösch, *Inorg. Chem.* **1997**, *36*, 3947; e) K. M. Neyman, V. A. Nasluzov, J. Hahn, C. R. Landis, N. Rösch, *Organometallics* **1997**, *16*, 995; f) K. L. Brown, N. Kaltsoyannis, *Dalton Trans.* **1999**, 4425; g) G. Christian, J. Driver, R. Stranger, *Faraday Discuss.* **2003**, *124*, 331.
[20] a) F. Maseras, M. A. Lockwood, O. Eisenstein, I. P. Rothwell, *J. Am. Chem. Soc.* **1998**, *120*, 6598; b) M. A. Lockwood, P. E. Fanwick, O. Eisenstein, I. P. Rothwell, *J. Am. Chem. Soc.* **1996**, *118*, 2762.
[21] a) F. Tuczek, N. Lehnert, *Angew. Chem.* **1998**, *110*, 2780; *Angew. Chem. Int. Ed.* **1998**, ***37***, 2636; b) N. Lehnert, F. Tuczek, *Inorg. Chem.* **1999**, *38*, 1659; c) N. Lehnert, F. Tuczek, *Inorg. Chem.* **1999**, *38*, 1671; d) K. H. Horn, N. Lehnert, F. Tuczek, *Inorg. Chem.* **2003**, *42*, 1076; e) N. Lehnert, B. E. Wiesler, F. Tuczek, A. Hennige, D. Sellmann, *J. Am. Chem. Soc.* **1997**, *119*, 8869.
[22] a) S. Khalal, J.-Y. Saillard, J.-R. Hamon, C. Manzur, D. Carrillo, *New J. Chem.* **2001**, *25*, 231; b) S. Khalal, J.-Y. Saillard, J.-R. Hamon, C. Manzur, D. Carrillo, *J. Chem. Soc. Dalton Trans.* **1998**, 1229.
[23] a) P. Schollhammer, E. Guenin, F. Y. Pétillon, J. Talarmin, K. W. Muir, D. S. Yufit, *Organometallics* **1998**, *17*, 1922; b) P. Schollhammer, B. Didier, N. Le Grand, F. Y. Pétillon, J. Talarmin, K. W. Muir, S. J. Teat, *Eur. J. Inorg. Chem.* **2002**, *3*, 658; c) F. Y. Pétillon, P. Schollhammer, J. Talarmin, K. W. Muir, *Inorg. Chem.* **1999**, *38*, 1954; d) N. Le Grand, K. W. Muir, F. Y. Pétillon, C. J. Pickett, P. Schollhammer, J. Talarmin, *Chem. Eur. J.* **2002**, *8*, 3115; e) F. Y. Pétillon, P. Schollhammer, J. Talarmin, K. W. Muir, *Coord. Chem. Rev.* **1998**, *178–180*, 203; f) P. Schollhammer, F. Y. Pétillon, S. Poder-Guillou, J. Y. Saillard, J. Talarmin, K. W. Muir, *Chem. Commun.* **1996**, 2633; g) J.-Y. Cabon, C. Le Roy, K. W. Muir, F. Y. Pétillon, F. Quentel, P. Schollhammer, J. Talarmin, *Chem. Eur. J.* **2000**, *6*, 3033; h) F. Y. Pétillon, P. Schollhammer, J. Talarmin, *J. Chem. Soc. Dalton Trans.* **1997**, 4019; i) F. Barriere, C. J. Pickett, J. Talarmin, *Polyhedron* **2001**, *20*, 27.
[24] a) D. Sellmann, A. Henninge, *Angew. Chem.* **1997**, *108*, 270; *Angew. Chem. Int. Ed. Engl.* **1997**, *36*, 276; b) M Reiher, O. Salomon, D. Sellmann, B. A. Hess, *Chem. Eur. J.* **2001**, *7*, 5195; c) D. Sellmann, J. Sutter, *Acc. Chem. Res.* **1997**, *30*, 460; d) S. Kuwata, Y. Mizobe, M. Hidai, *Inorg. Chem.* **1994**, *33*, 3619.
[25] ADF2002.01: a) E. J. Baerends, D. E. Ellis, P. Ros, *Chem. Phys.* **1973**, *2*, 42; b) G. te Velde, E. J. Baerends, *J. Comp. Physiol.* **1992**, *99*, 84.
[26] S. H. Vosko, L. Wilk, M. Nusair, *Can. J. Phys.* **1980**, *58*, 1200.
[27] A. D. Becke, *Phys. Rev. A* **1988**, *38*, 3098.
[28] J. P. Perdew, *Phys. Rev. B* **1986**, *33*, 8822.
[29] Gaussian 98, M. J. Frisch, G. W. Trucks, H. B. Schlegel, G. E. Scuseria, M. A. Robb, J. R. Cheeseman, V. G. Zakrzewski, J. Montgomery, J A, R. E. Stratmann, J. C. Burant, S. Dapprich, J. M. Millam, A. D. Daniels, K. N. Kudin, M. C. Strain, O. Farkas, J. Tomasi, V. Barone, M. Cossi, R. Cammi, B. Mennucci, C. Pomelli, C. Adamo, S. Clifford, J. Ochterski, G. A. Petersson, P. Y. Ayala, Q. Cui, K. Morokuma, D. K. Malick, A. D. Rabuck, K. Raghavachari, J. B. Foresman, J. Cioslowski, J. V. Ortiz, B. B. Stefanov, G. Liu, A. Liashenko, P. Piskorz, I. Komaromi, R. Gomperts, R. L. Martin, D. J. Fox, T. Keith, M. A. Al-Laham, C. Y. Peng, A. Nanayakkara, C. Gonzalez, M. Challacombe, P. M. W. Gill, B. G. Johnson, W. Chen, M. W.Wong, J. L. Andres, M. Head-Gordon, E. S. Replogle, J. A. Pople, Gaussian, Inc., Pittsburg, PA, **1998**.
[30] P. J. Hay, W. R. Wadt, *J. Chem. Phys.* **1985**, *82*, 299.

Received: June 8, 2004
Published online: November 10, 2004

  